Chemical Engineering & Processing: Process Intensification 120 (2017) 201–206

Contents lists available at ScienceDirect

Chemical Engineering & Processing: Process Intensification

journal homepage: www.elsevier.com/locate/cep

Synthesis of flower-shaped V_2O_5:Fe^{3+} microarchitectures in a high-gravity rotating packed bed with enhanced electrochemical performance for lithium ion batteries

Xiaochen Yang[a,b], Jingning Leng[a,b], Dan Wang[a,b,*], Zhiyong Wang[a,b], Jie-Xin Wang[a,b], Yuan Pu[a,b,*], Jianglan Shui[c], Jian-Feng Chen[a,b]

[a] State Key Laboratory of Organic-InorganicComposites, Beijing University of Chemical Technology, Beijing 100029, China
[b] Research Center of the Ministry of Education for High Gravity Engineering and Technology, Beijing University of Chemical Technology, Beijing 100029, China
[c] School of Materials Science and Engineering, Beihang University, Beijing 100191, China

ARTICLE INFO

Keywords:
High gravity rotating packed bed
Intensified mixing
Cathode materials
V2O5:Fe3+
Lithium-ion batteries

ABSTRACT

Flower-shaped microarchitectures of V_2O_5:Fe^{3+} were synthesized *via* an oxalic acid-assisted precipitation in a high-gravity rotating packed bed along with post hydrothermal and calcination process. The rotating packed bed (RPB) was used to create a high-gravity environment for V_2O_5:Fe^{3+} nanoparticles precipitation. Three dimensional (3D) micro-flowers were then formed due to the growth of V_2O_5:Fe^{3+} nanoplates and self-assembly during the hydrothermal and calcination process. As a result of the process intensification by high gravity technology, the V_2O_5:Fe^{3+} microarchitectures obtained by RPB were more uniform than those obtained in stirred tank, exhibiting excellent performance at high current density as cathode materials for lithium ion batteries (LIBs). This work put forward a novel method to control the crystal form of cathode materials for LIBs.

1. Introduction

Rechargeable lithium-ion batteries (LIBs) have been used in widespread applications, such as, hybrid electric vehicles (HEVs) and power electric vehicles (EVs) because of their high-energy density and environmental friendliness [1,2]. To meet the demand for high-performance LIBs, energy capacity, cycling stability and rate capability are the important factors to be concerned with. In order to improve battery performance,breakthroughs in electrode materials are critical [3–6]. Among the prospective cathode materials, vanadium pentoxide (V_2O_5) with a layered structure is a typical intercalation compound that has been extensively researched in the past decades [7,8]. When used as a Li-intercalation electrode, V_2O_5 has caught much attention owing to its essential advantages of high-energy density, high output voltage, abundant sources and low cost [9,10]. Within the potential range of 2.0–4.0 V (vs Li^+/Li), V_2O_5 has a high theoretical capacity of 294 mA h g^{-1} that is based on two Li-insertion per formula unit [5]. Nonetheless, due to its low Li-ion diffusion efficiency, poor structural stability and low electronic conductivity, the application of LIBs with V_2O_5 as a cathode material has been limited [11]. To date, to overcome the problems, one of the alternatives is to shorten diffusion distance and enlarge the electrode/electrolyte contact area. For the purpose, several groups prepared V_2O_5 with novel structures such as multidimensional nanomaterials, hollow microspheres and porous particles [12–17]. These materials were proved to show better electrochemical performance than the pristine V_2O_5.

Although novel V_2O_5 with nanostructures behaves excellent electrochemical performance, V_2O_5 shows low long-term cycling performance because of its poor structural stability, apparently. Eq. (1) is the reversible reaction. As x in $Li_xV_2O_5$ increases, V_2O_5 shows excellent cycling stability between 2.5 and 4.0 V which is corresponding to $0 < x < 1$. However, V_2O_5 always shows higher capacity fading than that in the range of 2.5–4.0 V, when the potential is lower than 2.5 V and extended to 2.0 V which is corresponding to $x > 1$. Generally, the method of introducing alien metal elements is used to improve electrical conductivities and cycling stability of V_2O_5 [18]. Particularly, many research literatures have proved that cationic doping is an effective way to increase the electrical conductivity, such as, Sn [19], Cu [20–23], Mn [2,24,25], Mo [26], Fe [27], Al [28], Nb and Ta [29], etc. Among these metal cations, Fe doped V_2O_5 is proved to enhance the structural stability during electrochemical cycling to a certain extent. As the cathode materials for LIBs, the uniform distribution of Fe^{3+} ions in V_2O_5 particles, is critical for the performance of LIBs. However, scalable preparation of V_2O_5 particles with uniform Fe^{3+} distribution is

* Corresponding authors at: State Key Laboratory of Organic-Inorganic Composites, Beijing University of Chemical Technology, Beijing, 100029, China.
E-mail addresses: wangdan@mail.buct.edu.cn (D. Wang), puyuan@mail.buct.edu.cn (Y. Pu).

http://dx.doi.org/10.1016/j.cep.2017.07.019
Received 30 June 2017; Received in revised form 15 July 2017; Accepted 20 July 2017
Available online 26 July 2017
0255-2701/

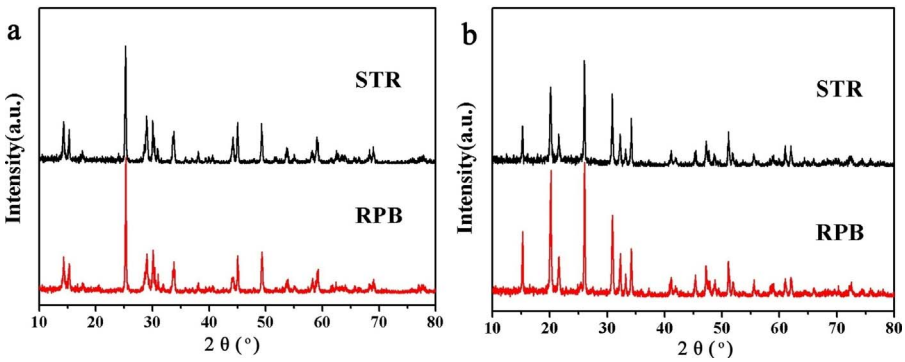

Fig. 1. The XRD patterns of the (a) precursor samples and (b) annealed samples.

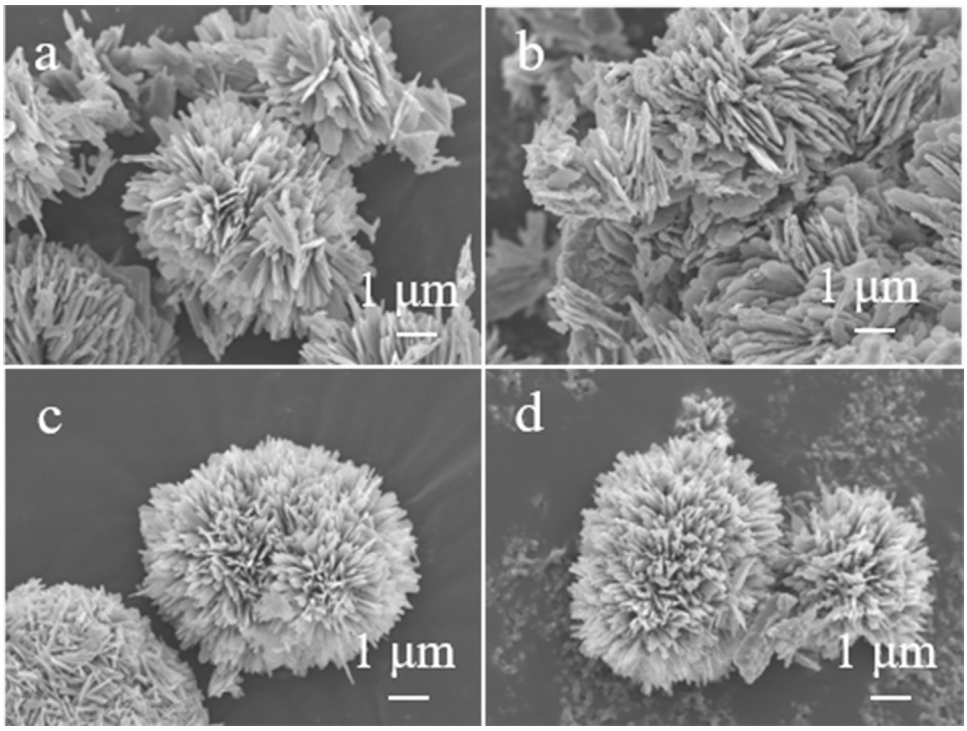

Fig. 2. Representative SEM images of nanoplate-assembled microspheres of precursor samples (a) STR, (b) RPB and annealed samples (c) STR, (d) RPB.

still challenging.

$$xLi^{+}+xe^{-}+V_2O_5 \leftrightarrow Li_xV_2O_5 \quad (1)$$

The rotating packed bed (RPB) reactor, which generates high-gravity environment, has been demonstrated as an efficient tool for homogeneous nucleation of particles [30–32]. Consequently, a variety of inorganic and organic nanoparticles with ultrafine size and uniform distribution have been prepared by RPB reactors [33–36]. However, as far as we are aware, the process intensification studies of using RPB reactors for producing V_2O_5 particles for LIBs applications have been rarely reported.

Herein, we report a novel route to prepare uniform micro-architectures of V_2O_5:Fe^{3+} by utilizing a RPB reactor for V_2O_5:Fe^{3+} nanoparticles precipitation, along with post hydrothermal and calcination process. The flower-shaped V_2O_5:Fe^{3+} microarchitectures are self-assembled by single-crystal nanoplates of V_2O_5:Fe^{3+}, with the sizes in the range of 100–200 nm. Due to the process intensification by high gravity technology, the V_2O_5:Fe^{3+} microarchitectures obtained by RPB are more uniform than those obtained in stirred tank. Their performance as cathode materials for LIBs is also investigated. The self-assembled flower-shaped V_2O_5:Fe^{3+} microarchitectures by RPB route exhibited good cycling stability in the voltage range of 2.4-4.0 V at high current density (5C).

2. Experimental section

2.1. Preparation of V_2O_5:Fe^{3+} microarchitechtures

All the chemical reagents were purchased form Sigma-Aldrich, Inc. and used as received. Deionized water was used in all the experimental procedures. For the synthesis of V_2O_5:Fe^{3+} in a RPB reactor, 0.6 g V_2O_5 and 0.9 g $H_2C_2O_4$ (molar ratio = 1:3) were mixed in 70 mL of deionized water under magnetic stirring at 80 °C for 20 min till a clear blue VOC_2O_4 solution was formed (solution A). 40 mg $Fe(NO_3)_3{\cdot}9H_2O$ were dissolved in 70 mL deionized water under magnetic stirring to form homogeneous solution of Fe^{3+} (solution B). After that, solution A and B were mixed in RPB reactor by the high gravity level β of 279 g. The high gravity level β of the RPB is determined by Eq. (2). More information could be seen in our previous work [37]. The obtained mixture solution from RPB were then transferred into 100 mL autoclaves and kept in an oven at 180 °C for 24 h. The precursors were washed and separated by centrifugation three times with ethanol and then dried at 80 °C. The final products of (RPB- V_2O_5:Fe^{3+}) were obtained after annealed at 500 °C for 2 h at a heating rate of 2 °C min^{-1}. As a control experiment, a stirred tank reactor (STR), which was composed of a beaker and a stirrer, was also used to mix the solution A and B. The V_2O_5:Fe^{3+} microarchitectures were then obtained following

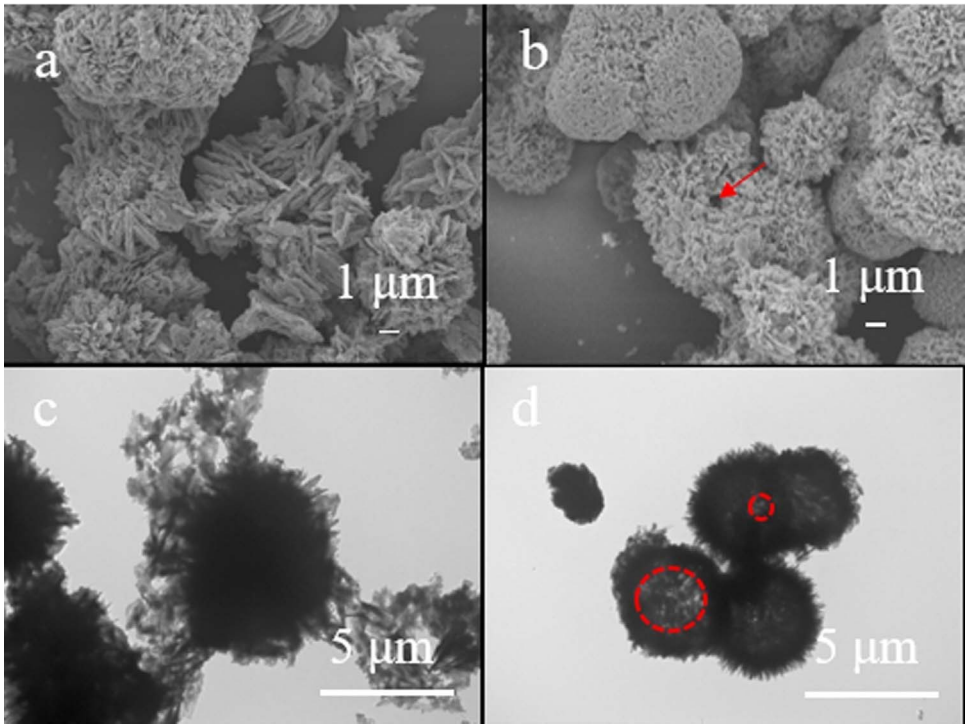

Fig. 3. Representative SEM images of nanoplate-assembled microspheres of annealed samples after ultrasonication (a) STR, (b) RPB and representative TEM images of annealed samples after ultrasonication (c) STR, (d) RPB.

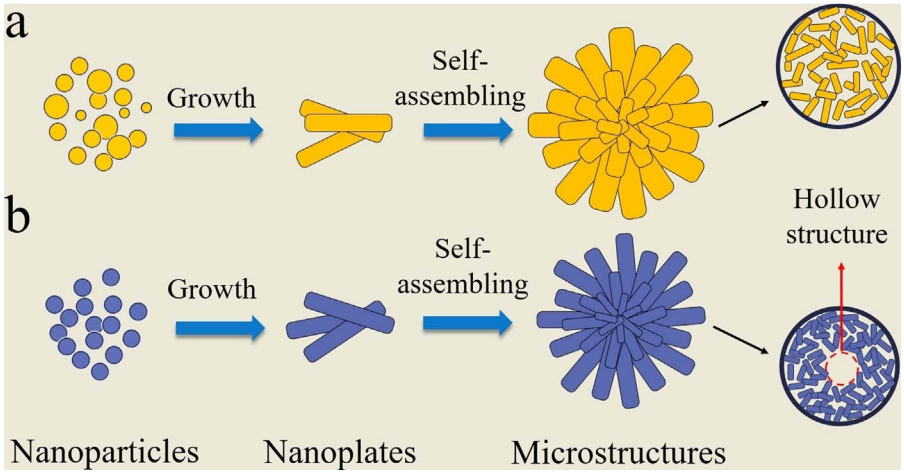

Fig. 4. Schematic illustration showing the evolution of nanoplate-assembled microstructures from nanoparticles (a) STR (b) RPB.

the same hydrothermal and calcination process (STR-V_2O_5:Fe^{3+}).

$$\beta = \frac{\omega^2 r}{g} \quad (2)$$

2.2. Characterizations

Crystallographic phases of all the samples were investigated by X-ray powder diffraction (Shimadzu, XRD-6000) at the 2θ range of 10°–80° using Cu Kα radiation. The morphologies of samples were examined by field emission scanning electron microscope (SEM, JEOL, JSM-6701F) at an acceleration voltage of 5.0 kV. The nanostructure was characterized using a Hitachi H-9500 transmission electron microscopy (TEM) operating at 300 kV in a bright-field mode. Theta Probe X-ray photoelectron spectroscopy (XPS, ESCALAB 250) was used to verify the valence state of vanadium and iron.

2.3. Electrochemical measurements

The electrochemical performances were investigated by assembly of 2032 coin cells in a glove box filled with pure argon gas. The working electrode slurry was prepared by dispersing V_2O_5:Fe^{3+} micro-architectures, super p and poly (vinylidene fluoride) (PVDF) binder in *N*-methyl-2-pyrrolidone (NMP) solvent with a weight ratio of 80:10:10, and the mass loading of the electrode materials is 1 mg/cm^2. Lithium plates were used as anode and 1 M solution LiPF6 in ethylene carbonate (EC)/dimethyl carbonate (DMC) were made up electrolyte. Galvanostatic charge/discharge cycling was tested in the voltage range of 4.0–2.4 V vs. Li/Li^+ with a multi-channel battery testing system (LAND CT2001A). Cyclic voltammetry (CV) was performed with an electrochemical workstation (VersaSTAT3).

3. Result and discussion

The preliminary analysis of the crystal structures of the precursor samples with Fe doping using different mixing methods were studied by

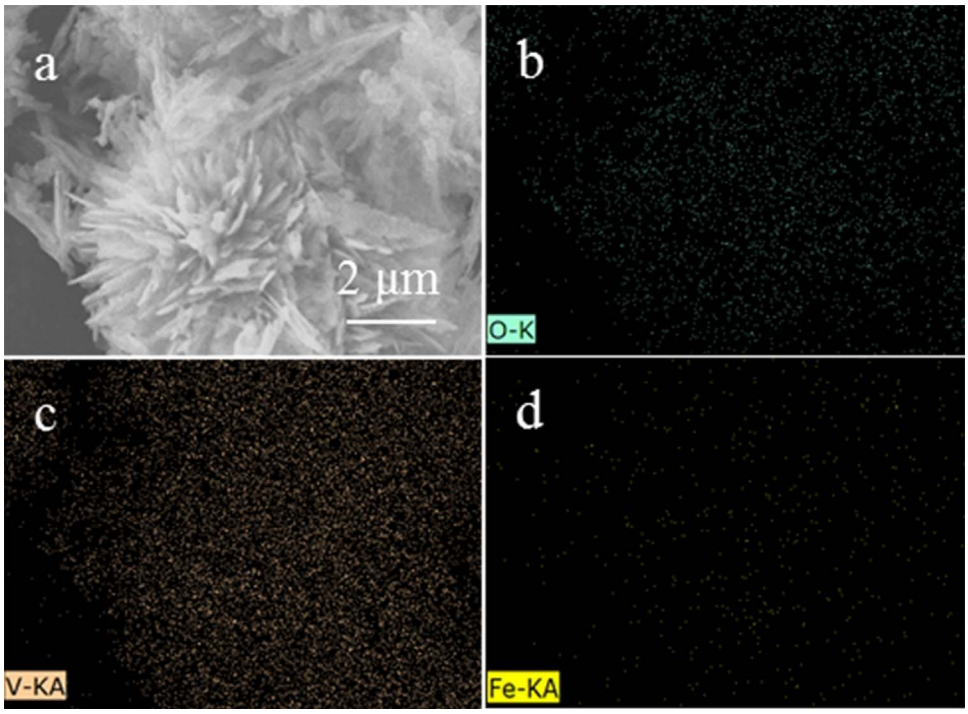

Fig. 5. EDS mapping of the annealed samples V_2O_5:Fe^{3+}.

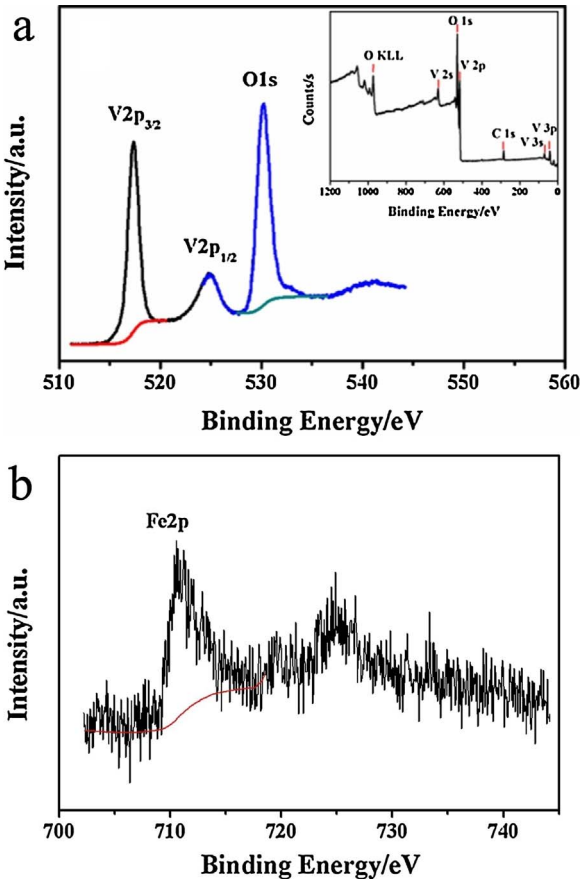

Fig. 6. The corresponding XPS spectra for sample V_2O_5 (a) the O1s and V2p bands, and (b) the Fe2p bands. The inset is the XPS wide-scan survey.

XRD. As shown in Fig. 1a, both precursors obtained by RPB approached and STR approach followed hydrothermal treatment exhibited the same crystal pattern of monoclinic VO_2 (JCPDS No. 81-2392). After annealing the precursors at 500 °C for 2 h, the monoclinic VO_2 transferred to V_2O_5. As the results shown in Fig. 1b, the XRD patterns of two samples matched well with the pattern of orthorhombic V_2O_5 (JCPDS No. 41-1426).

Fig. 2a and b showed the SEM images of VO_2:Fe^{3+} microarchitectures obtained by STR and RPB, respectively. Both samples exhibited flower-shaped structures with interconnected nanoplate subunits. The microarchitectures showed average diameter of 5 μm and the nanoplates was about 1 μm in length and 200 nm in width. It was noticed that the particles obtained by RPB approach were more uniform than those obtained by STR approach, which was attributed to the process intensification by high gravity technology during the nucleation of particles. The SEM images of V_2O_5:Fe^{3+} were presented in Fig. 2c and d respectively. It was observed that the morphologies of V_2O_5:Fe^{3+} by STR approach were irregular, with significant aggregated of the subunits. However, the V_2O_5:Fe^{3+} microarchitectures obtained by RPB approach exhibited similar flower-shaped structure as the VO_2:Fe^{3+} precursors. As RPB can create high-gravity environment by the centrifugal force, hence, very thin liquid films and/or tiny droplets are generated and the interface between liquid/liquid is renewed violently [38]. These results (Fig. 2b and d) demonstrated that RPB intensified the micro-mixing, which enabled the homogeneous nucleation and growth of particles.

The SEM and TEM images of V_2O_5:Fe^{3+} after ultrasonication were presented in Fig. 3 to further demonstrate the function of RPB. It was showed that the interior of V_2O_5:Fe^{3+} by STR approach was assembled by nanoplates irregularly and loosely. However, the interior of V_2O_5:Fe^{3+} by RPB approach was interconnected by tiny nanoplates compactly as the increasing contact opportunity among droplets created by RPB. Besides, some hollow structures with different sizes were found and it was assumed that the contact chance between droplets and air improved after RPB treatment resulting in the gas increase in the system. Subsequently, the gas escaped in the hydrothermal process and hollow structures formed. The illustration for the evolution of nanoplates formation and self-assembled microstructures using two different mixing methods of STR and RPB was shown in Fig. 4.

The results of energy dispersive spectrometry (EDS) mapping of V_2O_5:Fe^{3+} microarchitectures presented in Fig. 5. The three elements V, O and Fe in the mapping confirm the presence of Fe and V_2O_5. In

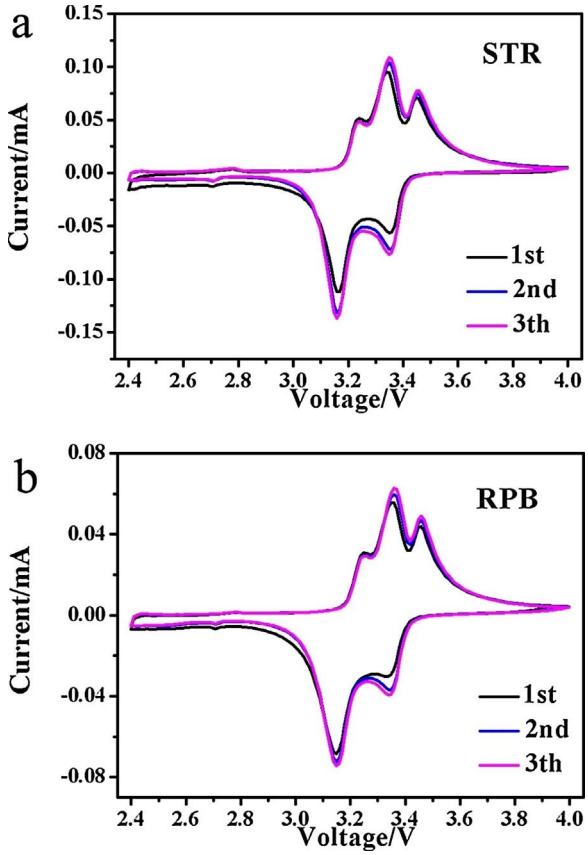

Fig. 7. CV curves of two electrodes between 2.4 and 4.0 V at a scan rate of 0.1 mV s^{-1} during the first three cycles (a) STR and (b) RPB.

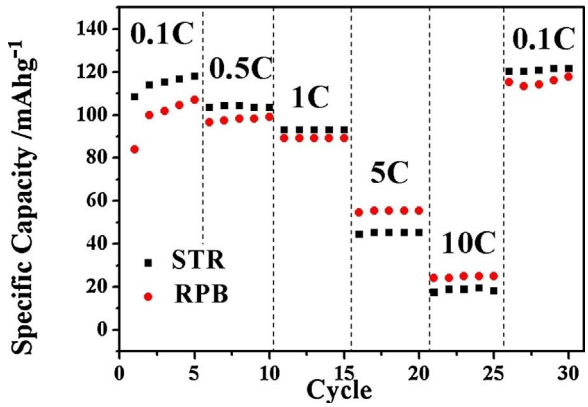

Fig. 8. Comparison of the rate capability of two electrodes at current densities from 0.1C to 10C.

addition, Fe is dispersed uniformly in the whole sample suggesting the homogeneously Fe doping in V_2O_5 particles is successful.

Furthermore, the oxidation of V and Fe was tested by X-ray photoelectron spectroscopy (XPS) analysis (Fig. 6). It reveals that the binding energy of $V2p_{3/2}$ at 517.3 eV can be assigned to V^{5+} and the binding energy of $Fe2p_{3/2}$ located at 710.6 eV is similar to that observed in Fe_2O_3 [39]. Accordingly, the oxidation states of V and Fe in the sample V_2O_5 are +5 and +3, respectively.

A series of comparative electrochemical measurements were performed by assembling coin cells with lithium plate as an anode to investigate the cathode performance of the samples. Fig. 7 showed the cyclic voltammograms (CV) of the two electrodes at a scan rate of 0.1 mV s^{-1} in the voltage range of 2.4–4.0 V during the first three cycles. The cathodic and anodic peaks in two patterns are related to the lithium ion insertion and extraction, respectively. Both V_2O_5:Fe^{3+}-STR and V_2O_5:Fe^{3+}-RPB electrodes exhibited two dominant cathodic peaks appear at around 3.34 and 3.15 V corresponding to a series of phase transformations from α-V_2O_5 to ε-$Li_{0.5}V_2O_5$ and δ-LiV_2O_5 during lithium ion intercalation into the V_2O_5 crystal (Eqs. (3) and (4) [40,41].

$$V_2O_5+0.5Li^++0.5e^- = Li_{0.5}V_2O_5 \quad (3)$$

$$Li_{0.5}V_2O_5+0.5Li^++0.5e^- = LiV_2O_5 \quad (4)$$

During the subsequent anodic process, for the two electrodes, two peaks located at 3.24 and 3.46 V were ascribed to the extraction of one lithium ion, forming $Li_{0.5}V_2O_5$ and V_2O_5, respectively. Apart from above mentioned two peaks, another peak located at around 3.35 V was observed for both two electrodes. Although the potential was controlled between 2.4–4.0 V which can decreased the irreversible phase transition that V_2O_5 undergoes upon polarization to 2 V (Li/Li^+), the cyclic voltammograms measurements of the two electrodes still showed irreversible structural changes [42]. In the subsequent scans, there were little changes of the current and peak areas for the whole process implies a stable structure of V_2O_5:Fe^{3+} microarchitectures. Fig. 8 shows the rate capability of the two electrodes at various current densities from 0.1C to 10C (1C = 294 mA g^{-1}). Compared with V_2O_5:Fe^{3+}-RPB, the V_2O_5:Fe^{3+}-STR electrode exhibits excellent rate performance at low current densities, such as, 01C, 0.5C, and 1C. However, when the current density enhanced to 5C, the rate performance of V_2O_5:Fe^{3+}-RPB electrode was better than that of V_2O_5:Fe^{3+}-STR electrode. It was assumed that the surface morphology of V_2O_5:Fe^{3+}-RPB electrode materials obtained by the RPB approached was benefit for lithium ion insertion and extraction at high current density. The lower rate capability of V_2O_5:Fe^{3+}-RPB electrode than V_2O_5:Fe^{3+}-STR electrode at low current density (< 5C), was attributed to the uniform and intense interior of V_2O_5:Fe^{3+}-RPB that impeded the embedded process of lithium ion. The SEM and TEM results in Fig. 3 can prove the assumption.

Fig. 9 shows the subsequent cycling performances at 5C, both two kinds of electrodes exhibited excellent cycling stability due to Fe doping in V_2O_5 particles. Fe^{3+} can act as a stabilizing agent by delay the phase transition resulting in enhancing the structural stability during electrochemical cycling [27,43]. Besides, the potential was controlled between 2.4–4.0 V which can decreased the irreversible phase transition. However, V_2O_5:Fe^{3+}-RPB electrode materials showed higher capacity than V_2O_5:Fe^{3+}-STR electrode materials.

4. Conclusion

We reported a novel route to prepare uniform microarchitectures of V_2O_5:Fe^{3+} by using a RPB reactor for V_2O_5:Fe^{3+} nanoparticles precipitation, along with post hydrothermal and calcination process. Due to the process intensification by high gravity technology, the V_2O_5:Fe^{3+} microarchitectures obtained by RPB were more uniform than those obtained in stirred tank. Their performance as cathode materials for LIBs was also investigated. The self-assembled flower-shaped V_2O_5:Fe^{3+} microarchitectures by RPB route exhibited good cycling stability in the voltage range of 2.4–4.0 V at high current density (5C). This work made a significant improvement to control the crystal form of cathode materials for LIBs at a large scale.

Acknowledgements

We are grateful for financial support from National Key Research and Development Program of China (2017YFB0404302 and 2017YFB0404300), the National Natural Science Foundation of China (51641201 and 21622601), the Fundamental Research Funds for the Central University (BUCTRC201601), and the “111” project of China (B14004).

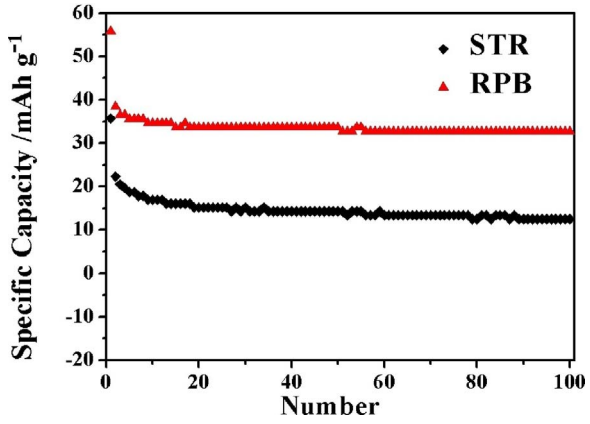

Fig. 9. Cycling performance (discharge capacity) of the two electrodes for 100 cycles at 5C.

References

[1] J. Xu, Y. Chen, L. Dai, Efficiently photo-charging lithium ion battery by perovskite solar cell, Nat. Commun. 6 (2015) 8103.

[2] J. Xu, Y. Lin, J.W. Connell, L. Dai, Nitrogen-doped holey graphene as anode for lithium ion batteries with high volumetric energy density and long cycle life, Small 11 (2015) 6179–6185.

[3] J. Xu, I.-Y. Jeon, J.M. Seo, S. Dou, L. Dai, J.-B. Baek, Edge-selectively halogenated graphene nanoplatelets (XGnPs, X = Cl, Br, or I) prepared by ball-milling and used as anode materials for lithium-ion batteries, Adv. Mater. 26 (2014) 7317–7323.

[4] J. Xu, S. Dou, H. Liu, L. Dai, Cathode materials for next generation lithium ion batteries, Nano Energy 2 (2013) 439–442.

[5] J. Shao, X.Y. Li, Z.M. Wan, L.F. Zhang, Y.L. Ding, L. Zhang, Q.T. Qu, H.H. Zheng, Low-cost synthesis of hierarchical V_2O_5, microspheres as high-performance cathode for lithium-ion batteries, ACS Appl. Mater. Interfaces 5 (2013) 7671–7675.

[6] J. Xu, I. Jeon, H. Choi, S. Kim, N. Park, L. Dai, J.-B. Baek, Metalated graphene nanoplatelets and their uses as anode materials for lithium-ion batteries, 2D Mater. 4 (2017) 014002.

[7] S.Q. Wang, Z.D. Lu, D. Wang, C.G. Li, C.H. Chen, Y.D. Yin, Porous monodisperse V_2O_5 microspheres as cathode materials for lithium-ion batteries, J. Mater. Chem. 21 (2011) 6365–6369.

[8] C. O'Dwyer, V. Lavayen, D.A. Tanner, B.S. Newcomb, E. Benavente, G. González, M.C. Sotomayor Torres, Reduced surfactant uptake in three dimensional assemblies of VO_x nanotubes improves reversible Li^+ intercalation and charge capacity, Adv. Funct. Mater. 19 (2009) 1736–1745.

[9] A.Q. Pan, H.B. Wu, L. Yu, T. Zhu, X.W. Lou, Synthesis of hierarchical three-dimensional vanadium oxide microstructures as high-capacity cathode materials for lithium-ion batteries, ACS Appl. Mater. Interfaces 4 (2012) 3874–3879.

[10] A.Q. Pan, T. Zhu, H.B. Wu, X.W. Lou, Template-free synthesis of hierarchical vanadium-glycolate hollow microspheres and their conversion to V_2O_5 with improved lithium storage capability, Chem. Eur. J. 19 (2013) 494–500.

[11] R.X. Yu, C.F. Zhang, Q. Meng, Z.X. Chen, H.K. Liu, Z.P. Guo, Facile synthesis of hierarchical networks composed of highly interconnected V_2O_5 nanosheets assembled on carbon nanotubes and their superior lithium storage properties, ACS Appl. Mater. Interfaces 5 (2013) 12394–12399.

[12] L.Q. Mai, L. Xu, C.H. Han, X. Xu, Y.Z. Lou, S.Y. Zhao, Y.L. Zhao, Electrospun ultralong hierarchical vanadium oxide nanowires with high performance for lithium ion batteries, Nano Lett. 10 (2010) 4750–4755.

[13] D.M. Yu, C.G. Chen, S.H. Xie, Y.Y. Liu, K. Park, X.Y. Zhou, Q.F. Zhang, J.Y. Li, G.Z. Cao, Mesoporous vanadium pentoxide nanofibers with significantly enhanced Li-ion storage properties by electrospinning, Energy Environ. Sci. 4 (2011) 858–861.

[14] C.F. Zhang, Z.X. Chen, Z.P. Guo, X.W. Lou, Additive-free synthesis of 3D porous V_2O_5 hierarchical microspheres with enhanced lithium storage properties, Energy Environ. Sci. 6 (2013) 974–978.

[15] E. Uchaker, N. Li, Y.W. Zhou, G.Z. Cao, Polyol-mediated solvothermal synthesis and electrochemical performance of nanostructured V_2O_5 hollow microspheres, J. Phys. Chem. C 117 (2013) 1621–1626.

[16] Y.S. Hu, X. Liu, J.O. Müller, R. Schlögl, J. Maier, D.S. Su, Synthesis and electrode performance of nanostructured V_2O_5 by using a carbon tube-in-tube as a nanoreactor and an efficient mixed-conducting network, Angew. Chem. Int. Ed. 48 (2009) 210–214.

[17] H.C. Pang, P. Cheng, H.B. Yang, J.L. Lu, C.X. Guo, G.L. Ning, C.M. Li, Template-free bottom-up synthesis of yolk-shell vanadium oxide as high performance cathode for lithium ion batteries, Chem. Commun. 49 (2013) 1536–1538.

[18] X. Huang, X.H. Rui, H.H. Hng, Q.Y. Yan, Vanadium pentoxide-based cathode materials for lithium-ion batteries: morphology control, carbon hybridization, and cation doping, Part. Part. Syst. Charact. 32 (2015) 276–294.

[19] Y.W. Li, J.H. Yao, E. Uchaker, M. Zhang, J.J. Tian, X.Y. Liu, G.Z. Cao, Sn-doped V_2O_5 film with enhanced lithium-ion storage performance, J. Phys. Chem. C 117 (2013) 23507–23514.

[20] H. Yu, X.H. Rui, H.T. Tan, J. Chen, X. Huang, C. Xu, W.L. Liu, D.Y.W. Yu, H.H. Hng, H.E. Hoster, Q.Y. Yan, Cu doped V_2O_5 flowers as cathode material for high-performance lithium ion batteries, Nanoscale 5 (2013) 4937–4943.

[21] H.X. Li, L.F. Jiao, H.T. Yuan, M. Zhao, M. Zhang, Y.M. Wang, High-performance Cu-doped vanadium oxide ($Cu_xV_2O_5$) prepared by rapid precipitation method for rechargeable batteries, Mater. Lett. 61 (2007) 101–104.

[22] Y.J. Wei, C.W. Ryu, K.B. Kim, Improvement in electrochemical performance of V_2O_5 by Cu doping, J. Power Sour. 16 (2007) 386–392.

[23] D. Zhu, H. Liu, L. Lv, Y.D. Yao, W.Z. Yang, Hollow microspheres of V_2O_5 and Cu-doped V_2O_5 as cathode materials for lithium-ion batteries, Scripta Mater. 59 (2008) 642–645.

[24] D.M. Yu, S.T. Zhang, D.W. Liu, X.Y. Zhou, S.H. Xie, Q.F. Zhang, Y.Y. Liu, G.Z. Cao, Effect of manganese doping on Li-ion intercalation properties of V_2O_5 films, J. Mater. Chem. 20 (2010) 10841–10846.

[25] H.M. Zeng, D.Y. Liu, Y.C. Zhang, K.A. See, Y.S. Jun, G. Wu, J.A. Gerbec, X.L. Ji, G.D. Stucky, Nanostructured Mn-doped V_2O_5 cathode material fabricated from layered vanadium jarosite, Chem. Mater. 27 (2015) 7331–7336.

[26] W. Yong, H.L. Zhang, H.T. Cao, T. Tian, J.H. Gao, L.Y. Liang, F. Zhuge, Effect of post-annealing on structural and electrochromic properties of Mo-doped V_2O_5 thin films, J. Sol-Gel Sci. Technol. 77 (2016) 604–609.

[27] S.R. Li, S.Y. Ge, Y. Qiao, Y.M. Chen, X.Y. Feng, J.F. Zhu, C.H. Chen, Three-dimensional porous $Fe_{0.1}V_2O_{5.15}$ thin film as a cathode material for lithium ion batteries, Electrochim. Acta 64 (2012) 81–86.

[28] K. Zhu, H.L. Qiu, Y.Q. Zhang, Y.Q. Zhang, D. Zhang, G. Chen, Y.J. Wei, Synergetic effects of Al^{3+} doping and graphene modification on the electrochemical performance of V_2O_5 cathode materials, ChemSusChem 8 (2015) 1017–1025.

[29] A. Sakunthala, M.V. Reddy, S. Selvasekarapandian, B.V.R. Chowdari, P. Christopher Selvin, Energy storage studies of bare and doped vanadium pentoxide, $(V_{1.95}M_{0.0}5)O_5$ M = Nb, Ta, for lithium ion batterie, Energy Environ. Sci. 4 (2011) 1712–1725.

[30] J.F. Chen, Y.H. Wang, F. Guo, X.M. Wang, C. Zheng, Synthesis of nanoparticles with novel technology: high-gravity reactive precipitation, Ind. Eng. Chem. Res. 39 (2000) 948–954.

[31] Y.Y. Kuang, Z.B. Zhang, M.L. Xie, J.X. Wang, Y. Le, Large-scale preparation of amorphous cefixime nanoparticles by antisolvent precipitation in a high-gravity rotating packed bed, Ind. Eng. Chem. Res. 54 (2015) 8157–8165.

[32] Q. Yang, J.X. Wang, F. Guo, J.F. Chen, Preparation of hydroxyapatite nanoparticles by using high-gravity reactive precipitation combined with hydrothermal method, Ind. Eng. Chem. Res. 49 (2010) 9857–9863.

[33] J. Leng, J. Chen, D. Wang, J.-X. Wang, Y. Pu, J.F. Chen, Scalable preparation of Gd_2O_3:Yb^{3+}/Er^{3+} upconversion nanophosphors in a high-gravity rotating packed bed reactor for transparent upconversion luminescent films, Ind. Eng. Chem. Res. (2017), http://dx.doi.org/10.1021/acs.iecr.7b02262.

[34] S. Shen, F. Gao, Y.B. Zhao, W. Wu, X.L. Yin, Preparation of high quality graphene using high gravity technology, Chem. Eng. Process. 106 (2016) 59–66.

[35] Q. Sun, B. Chen, X. Wu, M. Wang, C. Zhang, X.F. Zeng, J.X. Wang, J.F. Chen, Preparation of transparent suspension of lamellar magnesium hydroxide nanocrystals using a high-gravity reactive precipitation combined with surface modification, Ind. Eng. Chem. Res. 54 (2015) 666–671.

[36] B.Y. Lv, L.S. Zhao, Y. Pu, Y. Le, X.F. Zeng, J.F. Chen, N. Wen, J.X. Wang, Facile preparation of controllable-aspect-ratio hydroxyapatite nanorods with high-gravity technology for bone tissue engineering, Ind. Eng. Chem. Res. 56 (2017) 2976–2983.

[37] Z.Y. Wang, Z. Weng, M. Arowo, H.K. Zou, B.C. Sun, G.W. Chu, H. Zhao, J.F. Chen, Synthesis of heavy alkyl benzene sulfonate in a rotating packed bed combined with a stirred tank reactor, Chem. Eng. Process. 110 (2016) 123–127.

[38] H. Zhao, L. Shao, J.F. Chen, High-gravity process intensification technology and application, Chem. Eng. J. 156 (2010) 588–593.

[39] V.I. Nefedov, Y.V. Salyn, G. Leonhardt, R. Scheibe, A comparison of different spectrometers and charge corrections used in X-ray photoelectron spectroscopy, J. Electron. Spectrosc. Relat. Phenom. 10 (1977) 121–124.

[40] H.Q. Song, C.F. Liu, C.K. Zhang, G.Z. Cao, Self-doped V^{4+}-V_2O_5 nanoflake for 2 Li-ion intercalation with enhanced rate and cycling performance, Nano Energy 22 (2016) 1–10.

[41] Y.Z. Zheng, H.Y. Ding, E. Uchaker, X. Tao, J.F. Chen, Q.F. Zhang, G.Z. Cao, Nickel-mediated polyol synthesis of hierarchical V_2O_5 hollow microspheres with enhanced lithium storage properties, J. Mater. Chem. A 3 (2015) 1979–1985.

[42] M. Koltypin, V. Pol, A. Gedanken, D. Aurbach, The study of carbon-coated V_2O_5 nanoparticles as a potential cathodic material for Li rechargeable batteries, J. Electrochem. Soc. 154 (2007) A605–A613.

[43] J. Farcy, S. Maingot, P. Soudan, J.P. Pereira-Ramos, N. Baffier, Electrochemical properties of the mixed oxide $Fe_{0.11}V_2O_{5.16}$ as a Li intercalation compound, Solid State Ion. 99 (1997) 61–69.